

**GEOCHEMICAL INVESTIGATION OF SELECTED LAVA FLOWS
FROM MT. ETNA (ITALY)**

by

Ermanno Brosch & Christoph A. Hauzenberger

Institute of Earth Sciences, Department of Mineralogy and Petrology
University of Graz, Universitätsplatz 2, 8010 Graz, Austria

Abstract

Samples of selected lava flows from Mt. Etna volcano ranging from early submarine fissure type eruptions to the present day summit eruptions were investigated. Occurrence of tholeiitic basalts is restricted to the first period of activity of Mt. Etna volcano. Then a change in composition from tholeiitic to alkaline occurred. However, the compositions of these alkali basalts change over time from chemically evolved to less evolved/more primitive ones and vice versa. This suggests that fractional crystallisation and mixing of more primitive magma into the feeding system of Mt. Etna volcano played an important role in the differentiation of the samples. From major and trace element whole-rock analyses it is evident that all samples display typical fractionation trends resulting from removal of the major rock forming minerals such as plagioclase, olivine, clinopyroxene and Fe-Ti oxides and amphibole. Trace and REE element analyses obtained by LA-ICP-MS of cores and rims of plagioclase, olivine and clinopyroxene phenocrystals reveal that rims of some plagioclase grains grew in the presence of less evolved and therefore more primitive liquids. As for the magma source of Mt. Etna, it has been described to derive from an already slightly depleted garnet lherzolite. This assumption explains the observed depletion of HREE in whole rock chemical data as HREE are typically retained by a garnet lherzolite. Mt. Etna's erupted products have a within-plate basalt signature and display trace element similarities with Hawaiian volcanic rocks.

1. Introduction

Mt. Etna is located in the plain of Catania on the East coast of Sicily, the largest island of the Mediterranean Sea. Mt. Etna is a basaltic composite stratovolcano with a sub-rounded surface of 1180 km². It reaches a maximum diameter of about 45 km and a height of 3328 m (BRANCA et al., 2011). These dimensions make it the biggest active volcano in Europe. It is located above the convergent plate margin which extends between the African plate and the Eurasian plate. So Mt. Etna lies in a rather anomalous position on the Sicilian continental crust (CORREALE et al., 2014).

The Etna volcanic setting builds on the Gela-Catania sediments to South and Southeast, and on the Apenninic-Maghrebian sedimentary units to North and Northwest (DI STEFANO & BRANCA, 2002). Volcanism in the Etnean region began during the Middle Pleistocene and its most ancient eruption products are around 600 ka old (BRANCA et al., 2004). Over the course of the volcano's evolution there has been a shift from tholeiitic composition to alkaline composition. Extensive geological research has focussed on the evolutionary process of Mt. Etna leading to different evolution models. Numerous studies on Mt. Etna have been carried out. BRANCA et al. (2004) introduced the Supersynthem concept with the four evolutionary phases called Basal Tholeiitic-, Timpe-, Valle del Bove-, and Stratovolcano-Supersynthem (last one subdivided into Ellittico and Mongibello volcano) which represents the nowadays accepted subdivision for Mt. Etna.

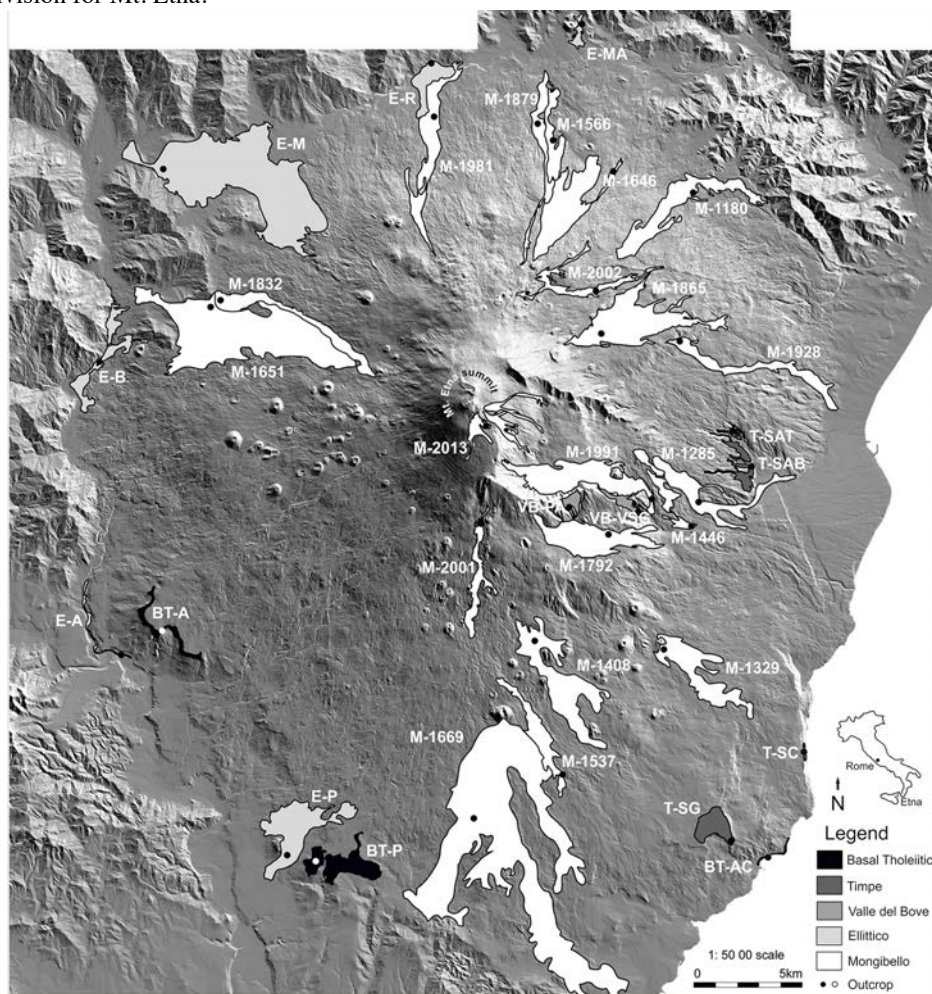


Fig. 1
Eruptions and outcrops map. All eruptions, except 2013, redrawn from BRANCA et al., 2011; eruption of 2013 redrawn from BEHNKE & DE BENI (2014). Digital elevation map of Mt Etna modified after PARESCHI et al., 1999.

In this work the samples were collected according to this subdivision.

This study presents a geochemical investigation of selected lava flows from Mt. Etna volcano. The various sampled lava flows were analysed focusing on whole-rock chemistry (major and trace elements) as well as trace element content in single minerals. These two aspects were combined and used to interpret changes during Mt. Etna's evolution over time such as lava flow compositions, evolution of magma with time and magmatic source.

2. Sampling and analytical methods

37 samples of chosen eruptions were collected from the study area ranging from the first fissure type eruptions located in Aci Castello to the most recent erupted ones at the summit (year 2013). The various sampled eruptions were chosen prior to field work by using the geological map of Mt. Etna volcano of 2011 issued by the National Institute of Geophysics and Volcanology (INGV) of Catania, Sicily (Italy). The collected samples cover an altitude range from 0 to 2800 m above sea level. Figure 1 presents a detailed map containing all sampled eruptions and the outcrops where the samples were collected. The names of the collected samples consist of the evolutionary phase they belong to (initials BT, T, VB, E and M) followed by the locality (initials) or year of eruption.

Mineral analyses were carried out at the Department of Mineralogy and Petrology, Institute of Earth Sciences at the University of Graz using a JEOL JSM-6310 scanning electron microscope (SEM) with a Link ISIS EDX spectrometer and Microspec WDX-600i spectrometer with an acceleration voltage of 15kV and a probe current of 6 nA. Fe_2O_3 was recalculated from FeO. Detection limit is 0.10 wt.%. Mineral analyses for ICP-MS were determined using a JEOL Superprobe JXA 8200 Electron Probe Microanalyzer (EPMA) at the UZAG Eugen-Stumpfl-Microprobe Laboratory (Univ. of Graz, Graz Univ. of Technology, Univ. Leoben) in Leoben. LA-ICP-MS analyses were carried out at the NAWI Graz Central Lab for Water, Minerals and Rocks (Univ. of Graz and Graz Univ. of Technology) using an Agilent ICP-MS 7500 coupled to an ESI Laser Ablation System NWR193.

Major and trace element analyses were carried out by ALS Global Laboratories in Spain using XRF, ICP-AES and ICP-MS.

3. Petrography and Mineral chemistry

All samples display a typical porphyritic texture, which can be subdivided into four categories (a) porphyritic ophimottled, (b) porphyritic seriate, (c) porphyritic seriate trachytic and (d) porphyritic microlithic seriate. The samples of each of the four Etnean evolutionary phases show features of minimum one to maximum three different textures at the same time. Basal Tholeiitic samples are the only ones displaying a porphyritic ophimottled texture (Figure 2a).

Porphyritic trachytic feature is displayed in Figure 2b by the Valle del Bove phase sample PA-2. In addition, plagioclase, amphibole and groundmass plagioclase display a fluidal texture. Sample E-M, taken in the locality of Maletto, belongs to the Ellittico volcano (Figure 2c) and shows a typical porphyritic seriate texture. Most of the samples featuring this texture however show differences in the groundmass components, mainly in the grain size and abundance of plagioclase. This can be observed in the sample of the 1566 eruption (Mongibello Volcano) in Figure 2d. In fact, a change in grain size of groundmass plagioclase can be noticed randomly.

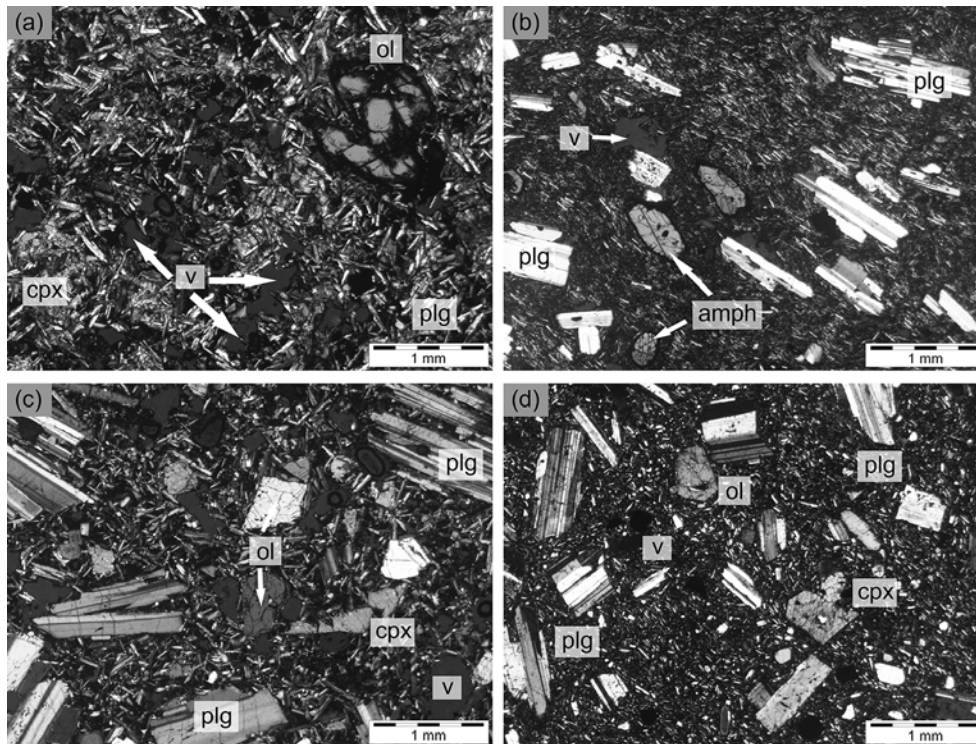


Fig. 2(a-d)

(a) Basal Tholeiitic porphyritic ophimottled texture; (b) Valle del Bove porphyritic trachytic texture; (c) Ellittico porphyritic seriate texture; (d) Mongibello porphyritic seriate texture. ol: olivine; plg: plagioclase; cpx: clinopyroxene; amph: amphibole; v: vesicle.

The collected samples are mainly composed of plagioclase, olivine and clinopyroxene. Minor minerals are potassium feldspar, amphibole, spinel, apatite, ilmenite and rare rutile, pyrite and chalcopyrite.

Plagioclase occurs both as phenocryst and as groundmass constituent. The grain size varies considerably ranging from <1 mm up to 2 cm. Typical polysynthetic twinning as well as optical zonation (e.g. oscillatory) are present. Plagioclase is mostly chemically zoned with decreasing anorthite component from core to rim. All plagioclase crystals are either labradorites or bytownites in composition with an average composition of An₆₅ to An₅₄ from core to rim. Table 1 shows representative plagioclase analyses.

Olivine, which is present as phenocrystals and as fine grains in the groundmass, shows grain sizes ranging from <1 mm to 5 mm. Iddingsitic alterations as well as fractures and holes can be noticed. Olivine shows chemical differences between core and rim with decreasing forsterite composition from core to rim. Average olivine composition found in all samples is Fo₇₅ to Fo₅₄ from core to rim. However, in some cases, olivines with increasing forsterite mol. % from core to rim were found. Table 2 contains selected olivine analyses.

Sample	BT-AC		T-SAB		VB-PA-1		E-B		M-1180	
	Basal Tholeiitic		Timpe		Valle del Bove		Ellittico		Mongibello	
	Core	Rim	Core	Rim	Core	Rim	Core	Rim	Core	Rim
SiO ₂	60,18	60,49	52,06	53,75	56,24	56,59	50,04	54,09	48,34	54,18
TiO ₂	0,20	0,15	0,14	0,26	0,15	0,16	<0,10	0,17	<0,10	<0,10
Al ₂ O ₃	24,74	24,61	29,82	29,32	27,25	26,90	31,85	28,31	32,34	28,26
Fe ₂ O ₃	<0,10	<0,10	<0,10	0,77	0,12	0,88	<0,10	<0,10	<0,10	<0,10
FeO	0,61	0,53	0,70	<0,10	0,47	<0,10	0,56	0,91	0,75	0,62
CaO	6,71	6,81	12,77	10,96	10,13	9,55	15,58	11,49	16,28	11,89
Na ₂ O	7,11	6,99	3,66	5,06	5,63	5,94	1,46	4,41	1,85	4,16
K ₂ O	0,37	0,31	0,25	0,22	0,40	0,48	<0,10	0,29	<0,10	0,30
Total	99,92	99,89	99,40	100,34	100,39	100,50	99,49	99,67	99,56	99,41

Normalization on the basis of 5 cations and 16 charges

Si	2,715	2,728	2,388	2,423	2,53	2,539	2,324	2,468	2,232	2,480
Ti	0,007	0,005	0,005	0,009	0,005	0,006	0,001	0,006	0,002	0,002
Al	1,316	1,308	1,612	1,557	1,444	1,422	1,744	1,523	1,761	1,524
Fe ³⁺	0,000	0,000	0,000	0,026	0,004	0,030	0,000	0,000	0,000	0,000
Fe ²⁺	0,024	0,020	0,027	0,000	0,018	0,000	0,022	0,035	0,029	0,024
Ca	0,324	0,340	0,628	0,529	0,488	0,459	0,775	0,562	0,805	0,583
Na	0,593	0,581	0,326	0,443	0,490	0,517	0,131	0,389	0,166	0,369
K	0,021	0,018	0,014	0,013	0,023	0,027	0,003	0,017	0,005	0,018
Total	5,000	5,000	5,000	5,000	5,000	5,000	5,000	5,000	5,000	5,000

Endmembers

X _{An}	0,335	0,343	0,649	0,538	0,487	0,458	0,852	0,580	0,825	0,601
X _{Ab}	0,643	0,638	0,336	0,450	0,490	0,515	0,144	0,403	0,170	0,381
X _{Or}	0,022	0,019	0,015	0,012	0,023	0,027	0,004	0,017	0,005	0,018

Tab. 1

Representative electron microprobe analyses of plagioclase in core and rim areas (wt.%).

Clinopyroxene occurs as well visible mineral grains reaching up to 2 mm in length, and in the fine-grained groundmass (< 0.1 mm). Typical twinning planes as well as zoning (sector and oscillatory) are present. Clinopyroxene is present as augite and pigeonite, the last one present only as small grains in the Basal Tholeiitic samples. Augites have a diopside rich composition. Chemical differences between core and rim as well as with other augites are present but are minimal compared to plagioclase or olivine. Average augite composition from core to rim is Wo₄₁₋₄₁En₄₅₋₄₃Fe₁₄₋₁₅. Pigeonite (average Wo₁₆₋₁₈En₅₅₋₅₃Fe₂₈₋₂₉ from core to rim) contains less Al₂O₃ and CaO but higher MgO and FeO. Table 3 contains representative pigeonite and augite clinopyroxene compositions.

4. Geochemistry

4.1. Whole-rock geochemistry

According to the TAS classification diagram of LE BAS et al. (1986) (Figure 3) the present investigated samples range from tholeiitic to alkaline basalts/trachyandesites (Representative whole-rock analyses in Table 4).

Sample	BT-A		T-SC		T-SG		E-P		M-1669	
	Basal Tholeiitic		Timpe		Timpe		Ellittico		Mongibello	
	Core	Rim	Core	Rim	Core	Rim	Core	Rim	Core	Rim
SiO ₂	40,05	39,45	38,87	38,74	38,59	37,29	36,84	37,14	38,89	38,27
TiO ₂	<0,10	<0,10	<0,10	<0,10	<0,10	<0,10	<0,10	<0,10	<0,10	<0,10
Cr ₂ O ₃	<0,10	<0,10	<0,10	<0,10	<0,10	<0,10	<0,10	<0,10	<0,10	<0,10
FeO	14,69	25,91	33,1	34,75	22,84	37,04	22,63	27,26	23,2	27,83
MnO	0,14	0,35	0,87	0,87	0,41	0,85	0,48	0,68	<0,10	0,53
MgO	44,25	33,34	26,71	25,15	37,46	24,16	39,11	34,21	36,86	33,05
CaO	<0,10	0,42	0,34	0,41	0,24	0,28	0,24	0,27	0,28	0,38
Total	99,13	99,47	99,89	99,92	99,54	99,62	99,30	99,56	99,23	100,06

Normalization on the basis of 3 cations (no Fe²⁺)

Si	1,012	1,060	1,085	1,091	1,015	1,062	0,962	0,996	1,024	1,028
Ti	0,001	0,000	0,001	0,001	0,000	0,000	0,002	0,000	0,001	0,001
Cr	0,001	0,000	0,000	0,000	0,000	0,000	0,001	0,001	0,001	0,000
Fe ²⁺	0,311	0,583	0,772	0,819	0,501	0,883	0,495	0,612	0,511	0,625
Mn	0,003	0,008	0,020	0,021	0,009	0,021	0,011	0,015	0,009	0,012
Mg	1,667	1,337	1,112	1,056	1,468	1,026	1,522	1,368	1,446	1,323
Ca	0,005	0,012	0,010	0,012	0,007	0,008	0,007	0,008	0,008	0,011
Total	3,000	3,000	3,000	3,000	3,000	3,000	3,000	3,000	3,000	3,000

Endmembers

X _{Mg}	0,843	0,696	0,590	0,564	0,745	0,538	0,755	0,691	0,739	0,680
X _{Fe}	0,157	0,304	0,410	0,436	0,255	0,462	0,245	0,309	0,261	0,320

Tab. 2

Representative electron microprobe analyses of olivine in core and rim areas (wt.%).

The alkaline rocks of the Timpe, Valle del Bove and Stratovolcano phase plot in the field of trachy-basalts, basaltic trachyandesites and trachyandesites. Figure 3 includes dark and light grey coloured areas which represent whole-rock analyses from literature of Etnean rocks of the same sampling areas. Published data for the various phases are as follows: For basal tholeiitic rocks: CRISTOFOLINI (1972) and TANGUY et al. (1997). For Timpe: BUSÀ (2002). For Valle del Bove: LOPEZ et al. (2006). For Ellittico: DEL CARLO et al. (2012). For Mongibello: CLOCCHIATTI et al. (2004), CORSARO & CRISTOFOLINI (1996), MÈTRICH et al. (2004), NICOTRA & VICCARO (2012) and TANGUY et al. (1997).

The change in chemistry from tholeiitic (Basal Tholeiitic phase) to alkaline for the subsequent following Timpe, Valle del Bove and Stratovolcano phase clearly shows that a change in the magma source occurred. Bivariate diagrams using mg# on the abscissa against selected major elements were used to display the chemical variation between the different lava flows. The major elements plot (Figure 4) shows clear differences between the tholeiites and the alkaline rocks. The tholeiites, which represent the oldest rocks, embody primitive basalts although their composition are slightly fractionated as mg# is below 65 in contrast to >70 for primitive basalts. The alkaline rocks display a more evolved composition with mg# varying from 58 to 38.

In general all samples display typical fractionation trends resulting from removal of the major rock forming minerals plagioclase, olivine and clinopyroxene as well as Fe-Ti oxides (such as spinel and ilmenite) and amphiboles in the alkaline rock suite.

Sample	BT-P		T-SAT		E-M		M-1537		M-2013	
	Basal Tholeiitic		Timpe		Ellittico		Mongibello		Mongibello	
	Core	Rim	Core	Rim	Core	Rim	Core	Rim	Core	Rim
SiO ₂	52,07	52,25	49,42	51,34	49,08	46,62	50,13	51,14	50,77	51,12
TiO ₂	0,74	0,75	1,19	1,07	1,83	2,88	1,32	1,19	1,17	1,22
Al ₂ O ₃	0,92	0,97	3,75	2,29	4,56	6,21	4,98	3,19	3,08	2,95
Cr ₂ O ₃	0,10	0,11	<0,10	<0,10	<0,10	<0,10	<0,10	<0,10	<0,10	<0,10
Fe ₂ O ₃	0,29	<0,10	4,81	2,94	2,55	3,08	1,19	<0,10	1,83	0,79
FeO	17,39	17,61	3,31	6,04	6,38	7,48	6,88	8,15	6,27	7,99
MnO	0,44	0,29	<0,10	0,31	0,26	0,24	0,12	0,21	0,17	0,21
MgO	19,31	18,35	15,28	15,00	13,39	12,01	14,05	14,52	14,79	14,46
CaO	7,70	8,99	21,43	20,92	21,05	20,44	20,92	20,66	21,26	20,65
Na ₂ O	0,14	0,10	0,45	0,52	0,59	0,64	0,48	0,33	0,37	0,36
K ₂ O	<0,10	<0,10	<0,10	<0,10	<0,10	<0,10	<0,10	<0,10	<0,10	<0,10
Total	99,10	99,42	99,64	100,43	99,69	99,60	100,07	99,39	99,71	99,75

Normalization on the basis of 4 cations and 12 charges

Si	1,959	1,968	1,960	1,965	1,914	1,899	1,956	1,944	1,940	1,943
Ti	0,021	0,021	0,026	0,024	0,051	0,081	0,038	0,034	0,033	0,034
Al	0,041	0,043	0,028	0,037	0,201	0,273	0,183	0,217	0,135	0,129
Cr	0,003	0,003	0,001	0,003	0,000	0,000	0,001	0,003	0,002	0,000
Fe ³⁺	0,008	0,000	0,007	0,000	0,000	0,000	0,000	0,000	0,000	0,000
Fe ²⁺	0,547	0,555	0,630	0,677	0,271	0,276	0,242	0,226	0,250	0,274
Mn	0,014	0,009	0,013	0,013	0,008	0,008	0,006	0,006	0,005	0,007
Mg	1,083	1,030	1,060	1,023	0,746	0,667	0,773	0,770	0,818	0,798
Ca	0,310	0,363	0,267	0,251	0,764	0,750	0,766	0,772	0,790	0,787
Na	0,011	0,007	0,008	0,007	0,043	0,046	0,035	0,028	0,027	0,026
K	0,003	0,001	0,000	0,000	0,002	0,000	0,000	0,000	0,000	0,002
Total	4,000	4,000	4,000	4,000	4,000	4,000	4,000	4,000	4,000	4,000

Endmembers

X_{Wo}	0,151	0,179	0,433	0,428	0,436	0,423	0,422	0,419	0,430	0,421
X_{En}	0,564	0,534	0,506	0,467	0,445	0,428	0,453	0,442	0,461	0,442
X_{Fs}	0,285	0,287	0,061	0,105	0,119	0,149	0,125	0,139	0,109	0,137

Tab. 3

Representative electron microprobe analyses of clinopyroxene (pigeonite and augite) in core and rim areas (wt.%).

Increasing SiO₂ with decreasing mg# indicates fractionation of olivine, clinopyroxene and partly Fe-Ti oxides. The decrease of CaO with increasing mg# is coupled with plagioclase and to a smaller extent to clinopyroxene fractionation. Al₂O₃ is incorporated into plagioclase, spinel and amphibole. For the alkaline rocks the decrease of TiO₂ and FeO_t over mg# can be explained by fractionation of Fe-Ti oxides such as spinels or ilmenite as well as probably Fe-rich amphiboles. K₂O and P₂O₅ which are neither incorporated into plagioclase nor into olivine or clinopyroxene, are also enriched in the remaining liquid.

In Figure 5 selected compatible and incompatible trace elements from whole-rock analyses were plotted against mg# displaying their behaviour with fractionation. All trace elements, except for Ni, show enrichment in the remaining liquid with increasing fractionation. Rb, Sr and Ba (LIL elements) show enrichment in the remaining liquid with increasing fractionation. This is also confirmed by their partition coefficients which are below 0.1 (ROLLINSON, 1993).

Sample	Basal Tholeiitic		Timpe		Valle del Bove		Ellittico		Mongibello			
	BT-AC	BT-A	T-SG	T-SAB	VB-PA-2	VB-VSG	E-P	E-R	M-1669	M-1792	M-1991	M-2013
SiO ₂	46.5	48.6	49.6	49.1	56.9	54.3	52.7	51.5	50	48.9	48.6	47.6
Al ₂ O ₃	13.7	13.95	17.75	19.65	19.3	19.15	18	18.65	18.1	16.95	16.7	17.25
Fe ₂ O ₃	11.7	11.85	10.55	9.17	5.93	7.77	9.49	9.32	10.15	10.9	11.2	11.45
CaO	8.14	9.23	9.41	9.61	5.26	6.9	6.6	7.98	10.15	9.67	10	9.99
MgO	10.15	9.59	5.39	3.29	1.79	2.75	3.17	2.89	4.87	5.13	5.38	4.86
Na ₂ O	2.8	3.1	4.13	4.36	5.87	5.62	5.81	4.68	3.85	4.04	3.95	3.84
K ₂ O	0.4	0.32	0.98	1.55	2.91	2.15	2.75	2.03	1.55	1.63	2	2.06
Cr ₂ O ₃	0.06	0.06	0.01	0.01	0.01	0.01	0.01	0.01	0.01	0.01	0.01	0.01
TiO ₂	1.48	1.45	1.48	1.42	0.79	1.25	1.64	1.5	1.49	1.6	1.68	1.67
MnO	0.16	0.15	0.16	0.16	0.15	0.16	0.18	0.17	0.17	0.18	0.18	0.18
P ₂ O ₅	0.25	0.27	0.36	0.56	0.41	0.71	0.89	0.7	0.52	0.53	0.56	0.58
SrO	0.04	0.05	0.11	0.16	0.14	0.19	0.11	0.17	0.14	0.13	0.14	0.15
BaO	0.01	0.02	0.05	0.08	0.12	0.1	0.12	0.11	0.07	0.08	0.08	0.08
LOI	5.77	0.22	0.02	0.04	0.74	0.33	0.44	0.37	0.09	0.12	0.35	0.14
Total	101.16	98.86	100	99.15	100.31	101.38	101.9	100.07	101.16	99.87	100.83	99.86
C	0.05	0.02	0.01	0.01	0.01	0.01	0.01	0.01	0.01	0.01	0.01	0.01
S	0.14	0.04	0.02	0.02	0.02	0.02	0.02	0.02	0.01	0.01	0.02	0.02
Ba	117	131	393	661	980	850	1010	891	637	659	681	667
Ce	34.9	36.4	62.7	116	157	167	182	157	113	119	117	116
Cr	460	480	100	10	20	10	20	10	50	40	30	20
Cs	0.07	0.06	0.41	0.57	1.06	0.62	1.16	0.39	0.59	0.67	0.83	0.91
Dy	4.24	3.88	4.3	5.2	4.47	5.35	6.31	6.01	5.11	5.49	5.72	5.91
Er	2.2	1.97	2.26	2.49	2.37	2.66	3.15	2.96	2.49	2.69	2.83	2.9
Eu	1.51	1.48	1.95	2.79	2.45	3.18	3.35	3.24	2.71	2.78	2.83	2.86
Ga	17.1	16.1	23.8	26.4	26.5	26.4	27.1	26	24	24.4	23.5	23.2
Gd	4.67	4.55	5.25	7.46	6.16	7.83	9.02	8.84	7.19	7.53	8.14	7.9
Hf	2.6	2.4	3.4	4.9	8.2	6.7	7.6	6.2	4.7	5.3	5.1	5.2
Ho	0.83	0.77	0.89	0.94	0.85	0.96	1.15	1.09	0.92	1	1.01	1.05
La	16.3	17.6	32.8	61.2	92.8	92.4	99.5	85.9	60.1	60.9	60.7	58.9
Lu	0.27	0.23	0.34	0.31	0.34	0.32	0.42	0.36	0.3	0.33	0.31	0.34
Nb	18.2	16.8	45.1	60.8	112	94.2	130	76.5	56.3	57.4	54.5	49.7
Nd	18.7	18.8	27.3	45.8	50.4	61.4	66.4	62.3	47.2	49.5	50.7	50.3
Pr	4.33	4.44	7.08	12.65	15.3	17.4	19	17	12.5	13.05	13.2	13.1
Rb	4.7	5.4	21.5	39.5	86.7	49.7	73.9	43.1	35	36.6	47.6	52.2
Sm	4.59	4.42	5.27	8.22	7.67	9.4	10.95	10.55	8.49	9.15	9.59	9.64
Sr	368	435	977	1545	1300	1710	1070	1485	1340	1225	1270	1295
Ta	0.9	0.8	2.2	2.9	5.7	4.5	6.2	3.6	2.6	2.7	2.5	2.4
Tb	0.67	0.66	0.85	0.97	0.85	1.01	1.18	1.12	0.98	1.01	1.04	1.05
Th	1.93	1.99	5.47	9.71	23.2	14.35	21.1	15.05	9.3	9.78	8.75	8.16
Tl	0.5	0.5	0.5	0.5	0.5	0.5	0.5	0.5	0.5	0.5	0.5	0.5
Tm	0.3	0.28	0.38	0.35	0.35	0.37	0.43	0.41	0.33	0.38	0.37	0.38
U	0.54	0.57	1.71	2.74	7.36	3.72	5.97	4.36	2.57	2.74	2.51	2.33
V	203	179	261	287	98	138	209	204	287	324	330	322
Y	20.7	18.9	21.7	25.5	23.7	26.1	31.2	28.9	24.7	26.4	27.4	27.6
Yb	1.79	1.7	2.07	2.18	2.38	2.21	2.73	2.44	2.06	2.24	2.33	2.38
Zr	97	89	151	241	451	359	398	291	228	246	237	238
Ag	<0.5	<0.5	<0.5	<0.5	<0.5	<0.5	<0.5	<0.5	<0.5	<0.5	<0.5	<0.5
Bi	0.25	0.01	0.02	0.03	0.02	0.03	0.02	0.01	0.02	0.03	0.02	0.02
Cd	<0.5	<0.5	<0.5	<0.5	<0.5	<0.5	<0.5	<0.5	<0.5	<0.5	<0.5	<0.5
Co	51	51	33	26	13	18	24	19	34	36	36	36
Cu	85	41	61	134	38	40	67	24	126	126	133	128
Hg	0.06	0.01	<0.01	<0.01	<0.01	<0.01	<0.01	<0.01	<0.01	<0.01	<0.01	<0.01
Li	<10	<10	<10	<10	<10	<10	<10	<10	<10	<10	<10	<10
Ni	190	182	41	8	2	3	3	2	22	19	22	15
Pb	9	3	7	7	13	12	12	10	9	10	10	6
Sb	0.52	0.12	0.2	0.19	0.29	0.31	0.2	0.17	0.11	0.15	0.09	0.37
Sc	27	25	19	13	4	7	11	11	19	22	22	21
Se	0.6	0.4	0.5	0.9	0.5	0.7	1	0.7	1.1	1	1.1	1
Te	0.01	<0.01	0.01	0.01	<0.01	0.01	0.01	0.01	0.01	<0.01	<0.01	0.01
Zn	109	104	89	96	98	103	110	102	96	101	100	100

Tab. 4

Representative whole-rock analyses (wt.% for major and ppm for trace elements).

On the other hand, Ni, which is a compatible element, shows a decrease with fractionation as it is incorporated into olivine and clinopyroxene with preference into the olivine structure (Partition coefficient of 14 compared to 7 for clinopyroxene; ROLLINSON, 1993).

Zr, Y, Ce and Eu (HFS elements) behave the same way as the above mentioned LIL elements. Thus the observed trends in Figure 5 show that the amount of incompatible elements increases in the remaining liquid due to crystal fractionation and removal of compatible elements from the liquid.

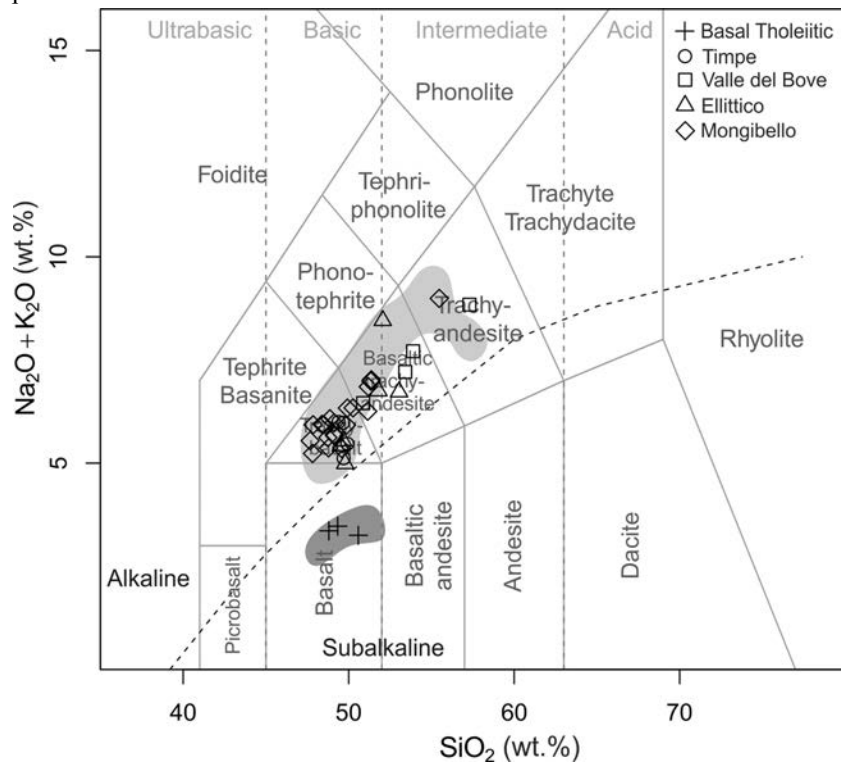


Fig. 3
TAS diagram of LE BAS et al. (1986) differentiating the collected samples into the fields of basalt, trachybasalt, basaltic trachyandesite and trachyandesite. Grey coloured area represents already published data of the same eruptions of the same eruptions of this study for a visual comparison.

Figure 6 shows a NMORB (SUN & MCDONOUGH, 1989) normalised plot (increasing incompatibility from left to right) of representative samples displaying an irregular pattern, which is common for all analysed samples and shows different degrees of enrichment between LILE (K and LREE) and HFS (Zr, Ti and HREE). Basal tholeiitic phase samples plot apart from the alkaline suite samples showing less abundance in all elements. The alkaline suite shows almost the same trend at elevated levels, however there is no systematic increase in concentration coupled to the evolutionary sequence: from the Timpe phase onwards there is an overall enrichment in trace element content with a sudden increase in the concentrations belonging to the Valle del Bove phase which are among the most evolved ones. After that a subsequent depletion of trace elements from Ellittico volcano to Mongibello volcano is observed. As suggested by CORSARO & CRISTOFOLINI (1996) and CORSARO & POMPILIO (2004) eruption products of Mt. Etna have trace element patterns close to within-plate basalts or ocean island basalts.

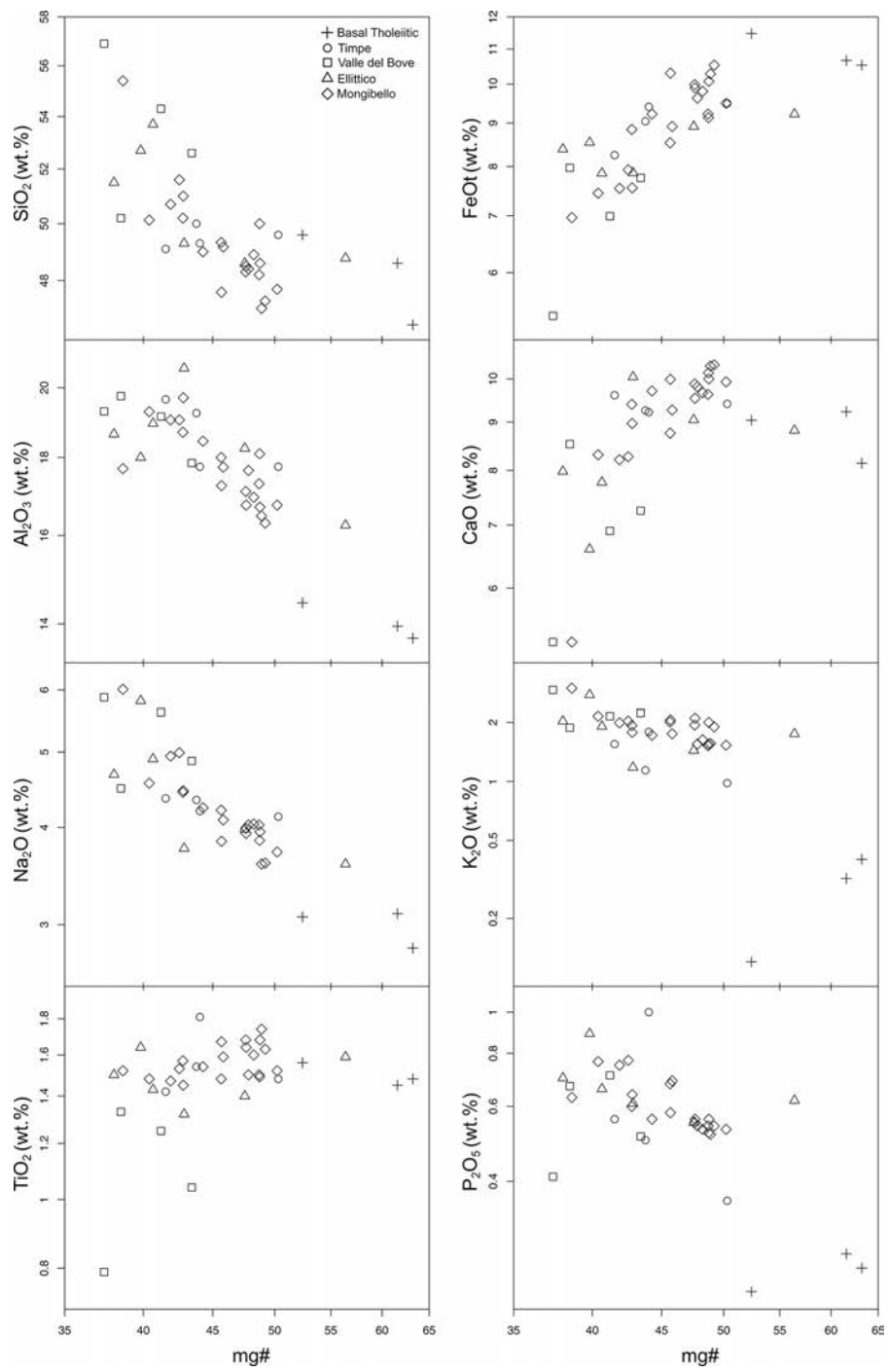


Fig. 4
Major elements bivariate diagrams for the Etean samples displaying fractionation trends.

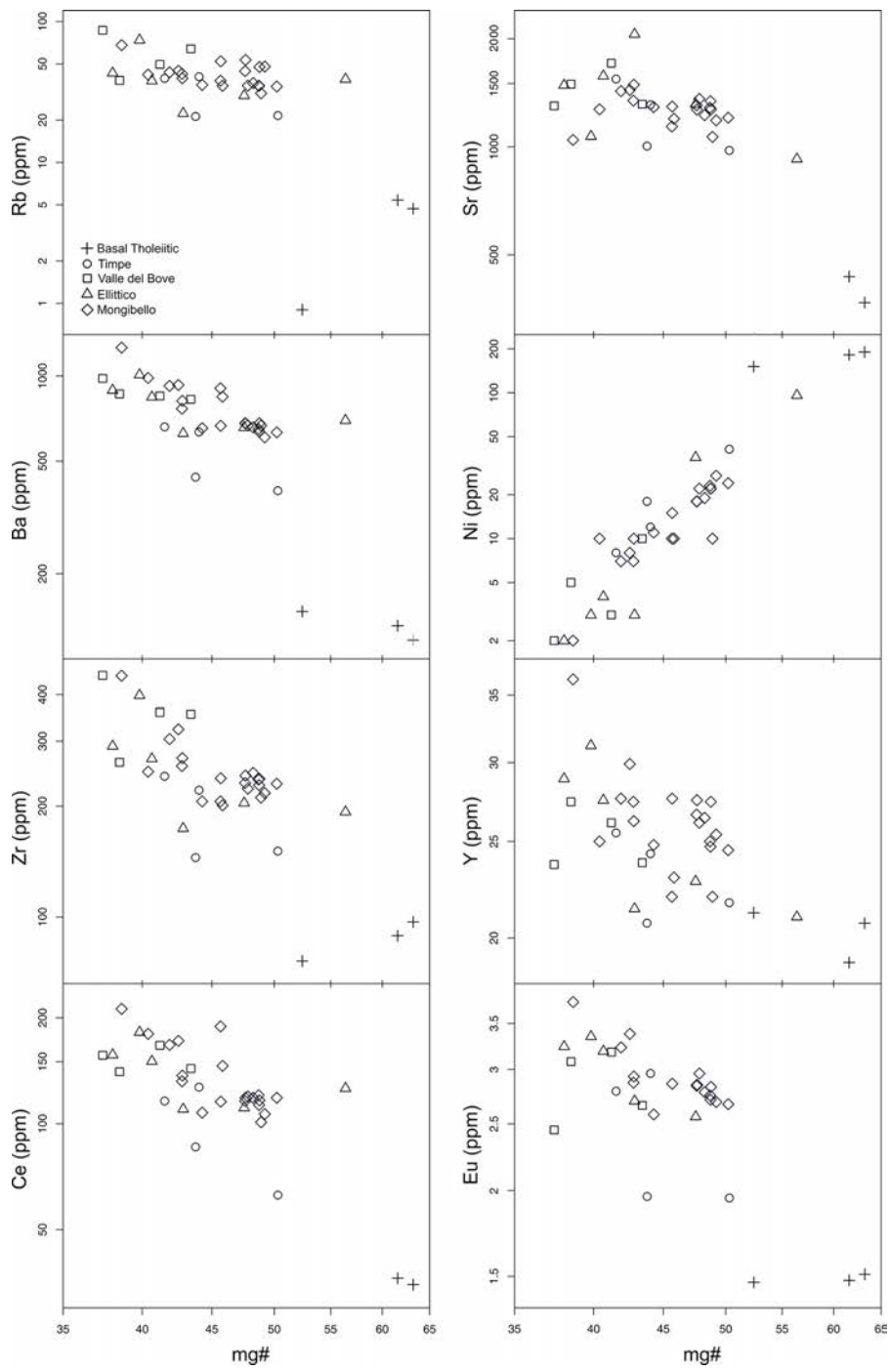


Fig. 5
Trace elements bivalent diagrams for the Etean samples displaying fractionation trends.

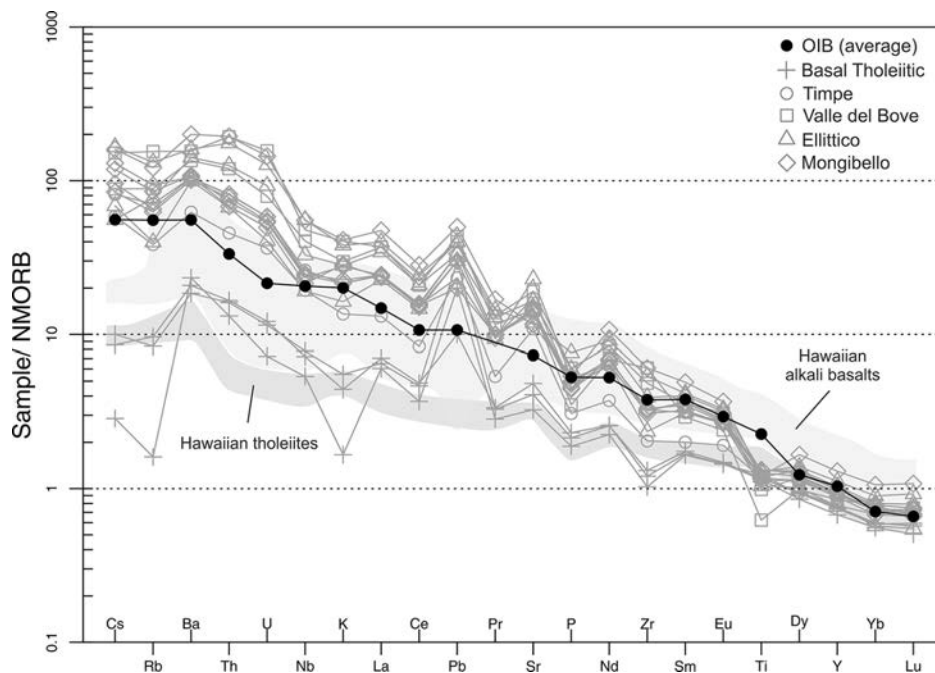


Fig. 6
 SUN & MCDONOUGH (1989) NMORB normalized plot of representative samples compared with a typical average within-plate basalt (SUN & MCDONOUGH, 1989) as well as selected tholeiitic and alkali basaltic compositions of Hawaiian volcanoes.

As a comparison, a typical average within-plate basalt (SUN & MCDONOUGH, 1989) as well as selected tholeiitic and alkali basaltic compositions from Hawaii [Kilauea, Mauna Kea and Mauna Loa; References: WEST et al. (1988), WANG et al. (1994), WANLESS et al. (2006), MARSKE et al. (2008) and SISSON et al. (2009)] were included into the diagram. Tholeiites as well as the alkaline rocks from Mt. Etna follow similar trends as observed from Hawaii. Both rock types are enriched in LILE and HFS elements compared to a MORB but display a number of differences in terms of different element concentrations (e.g. elements Pb, Sr, and Ti) compared to the average within-plate basalt.

Within the Ti-Zr discrimination diagram of PEARCE (1982) (Figure 7) the samples plot in the within-plate basalts and MORB type fields. For comparison, selected tholeiitic and alkali basaltic compositions from Hawaii (Kilauea, Mauna Kea and Mauna Loa; References same as before) were included into the diagram. This discrimination diagram confirms the within-plate basalt trace element pattern documented above.

4.2. Trace element geochemistry of single minerals

4.2.1. Plagioclase

In Figure 8 the trace elements Sr, Eu, Ba and Ce are plotted against X_{An} which is used as fractionation index for plagioclase. There is no linear increase or decrease of trace elements over time in concordance with the evolutionary sequence of Mt. Etna.

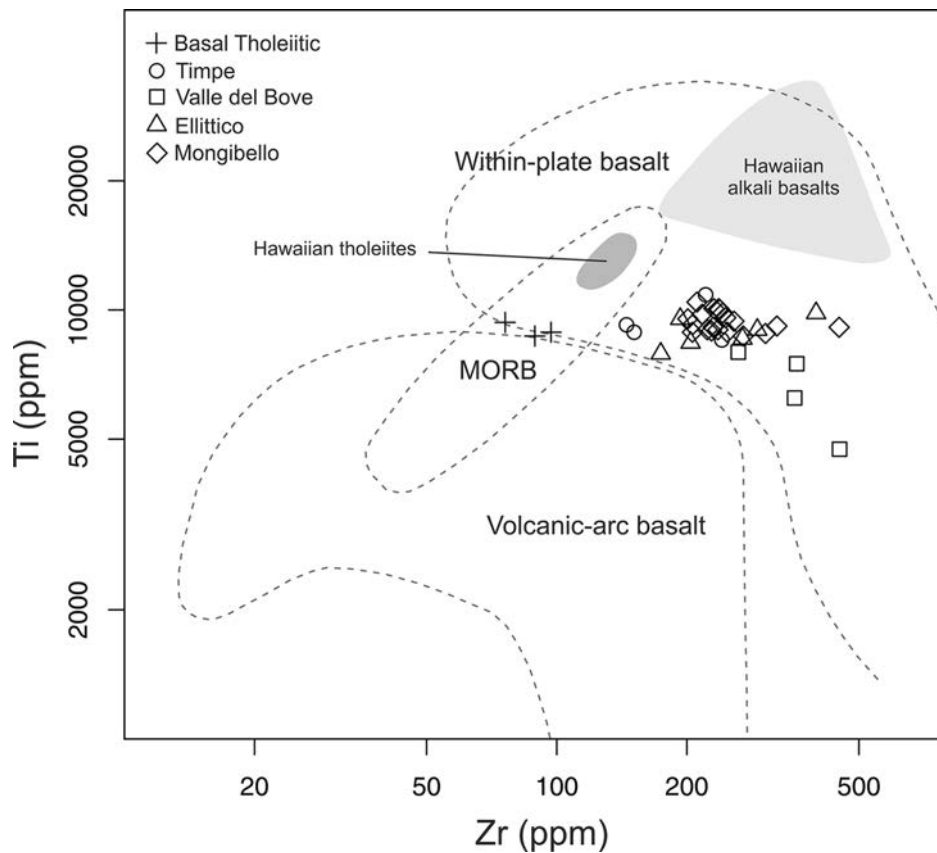


Fig. 7

Samples plotted on the Ti-Zr discrimination diagram of PEARCE (1982). Only tholeiitic samples plot in the MORB field while all alkali basalts plot in the within-plate basalt field. For comparison, tholeiitic and alkali basaltic compositions of Hawaiian volcanoes are included.

From the analyses in Table 5 it is evident that some plagioclase phenocrysts show inverse zonation. This is also clearly notable in Figure 8 where core analyses (full symbols) plot at lower X_{An} while rim analyses (open symbols) plot at higher X_{An} values. Sr is concentrated in plagioclase as it is preferentially incorporated into its structure rather than in olivine or clinopyroxene. Ba is found in a 35 to 450 ppm concentration range in plagioclase, again with no systematic core-rim relationship. Ce and Eu show great variability in the plagioclase analyses and follow basically the trend seen in Ba.

4.2.2. Olivine

Olivine bivariate plots using trace elements Cr, Ni, Li and Ti over mg# (Figure 9) display large differences between the olivine grains from the different evolutionary phases as well as between cores and rims (see Table 6 for representative analyses). There is a decrease in Cr and Ni with increasing fractionation. The tholeiitic sample BT-A contains olivines rich in Cr and Ni which indicates the rock's primitive nature.

Then with increasing fractionation olivines of the alkaline suites show an overall decrease in Ni and Cr. Ellittico sample E-R features a curious Ni anomaly having the absolute lowest Ni ppm content in all olivine analyses while at the same time it features the highest Li content.

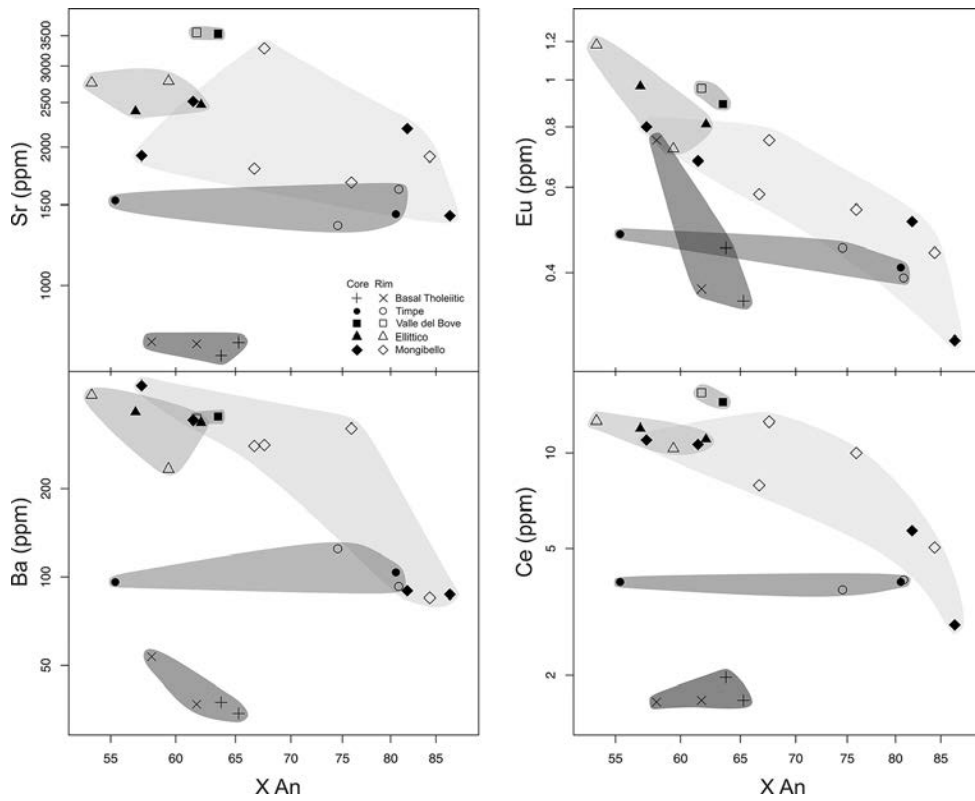


Fig. 8
Bivariant diagram of plagioclase core and rim ICP-MS analyses. Trace elements Sr, Eu, Ba and Ce are plotted against X_{An} which is used as fractionation index.

4.2.3. Clinopyroxene

Clinopyroxene shows great chemical variability with regard to trace elements as well as REE (Table 7). In Figure 10 the bivariant plots mg# versus Ni, Ti, Sr and Y for clinopyroxenes (cores and rims) reveal a number of trends. In the mg#-Ni plot the Ellittico sample E-R displays the lowest Ni contents for clinopyroxene. This is also observed for olivines of the same sample. As expected, the tholeiitic sample BT-A shows the highest Ni concentration at relatively high mg# for the core and a slightly lower Ni content at a more fractionated stage (lower mg#). Y and Ti show enrichment with fractionation. Sr decreases with fractionation and although incompatible in clinopyroxene it is to some extent included in its structure.

Sample	BT-A		T-SG		VB-VSG		E-R		M-1669		M-2013	
	Basal Tholeiitic		Timpe		Valle del Bove		Ellittico		Mongibello		Mongibello	
	Core	Rim	Core	Rim	Core	Rim	Core	Rim	Core	Rim	Core	Rim
SiO ₂	52.47	54.23	47.58	47.98	53.18	53.77	52.42	53.35	53.98	49.30	48.93	48.24
Al ₂ O ₃	29.37	28.44	32.78	32.83	28.87	28.64	30.89	29.87	29.61	33.08	32.45	33.03
FeO	0.39	0.31	0.65	0.72	0.29	0.31	0.67	0.54	0.72	0.70	0.49	0.78
MgO	0.19	0.13	0.07	<0.05	0.05	0.11	<0.05	0.03	<0.05	<0.05	0.26	0.08
CaO	12.97	11.58	15.87	15.70	12.58	12.26	11.98	11.49	11.14	14.86	15.91	16.33
Na ₂ O	3.75	4.55	2.11	1.98	3.84	4.06	3.86	4.11	4.28	2.50	1.91	1.63
K ₂ O	0.10	0.11	0.01	0.11	0.24	0.23	0.28	0.34	0.46	0.16	0.07	0.09
Total	99.24	99.35	99.07	99.32	99.05	99.38	100.1	99.73	100.19	100.6	100.02	100.18
Li	0.49	2.24	-0.45	0.55	<0.57	<0.52	<0.67	<0.75	0.67	<0.53	1.62	1.1
Be	0.13	0.13	0.24	0.21	0.34	0.36	0.61	0.32	0.29	0.3	0.16	0.28
Ti	318	451	302	293	363	347	434	333	473	372	167	135
V	1.92	3.97	1.21	1.43	0.75	0.68	1.84	1.43	1.91	3.38	0.95	0.85
Cr	<1.12	<0.97	<0.96	<0.98	<1.09	<1.08	<1.19	<1.38	<0.95	<0.92	<1.12	<0.85
Mn	25.7	23	25.7	33	28.5	31	30	35.4	20.1	22	29.3	24.2
Co	0.91	0.85	0.31	0.26	0.39	0.32	0.51	0.28	0.73	0.82	0.44	0.44
Ni	0.74	0.61	0.27	0.41	0.44	0.38	0.48	0.43	0.39	0.36	0.69	0.32
Cu	2.98	1.04	1.94	1.59	<0.29	0.31	1.29	<0.34	<0.24	2.94	1.06	1.51
Zn	4.58	9.14	3.51	2.47	4.36	4.09	4.77	4.04	4.17	4.35	2.89	2.61
Ga	21.4	25.5	22.5	22.3	25.8	25.4	28.4	29.5	25.4	28	26.7	22.6
Ge	0.74	0.78	0.64	0.79	0.66	0.57	0.99	0.59	0.74	0.59	0.4	0.42
Rb	0.19	0.25	0.21	0.17	0.43	0.32	0.73	<0.20	1.08	1.04	<0.16	<0.12
Sr	753	756	1432	1620	3527	3552	2474	2787	1916	1676	2197	1907
Y	0.14	0.18	0.15	0.17	0.23	0.2	0.23	0.24	0.18	0.2	0.16	0.15
Zr	0.11	0.15	0.17	0.09	0.09	0.08	0.4	0.05	0.1	0.69	0.03	<0.02
Nb	0.01	0.01	0.02	0.03	0.01	<0.01	0.06	0.03	0.01	0.16	0.01	<0.01
Cs	<0.12	<0.11	<0.11	<0.11	<0.14	<0.13	<0.16	<0.18	<0.13	<0.13	<0.14	<0.12
Ba	34.2	53.6	104	92.7	352	346	336	233	449	321	89.7	84.9
La	1.27	1.41	3.39	3.02	13.1	13.9	9.13	8.42	10.3	9.75	4.31	4.28
Ce	1.67	1.65	3.93	3.99	14.5	15.5	11.1	10.3	11	9.99	5.7	5.04
Pr	0.18	0.19	0.36	0.37	1.33	1.32	0.98	0.88	0.82	0.69	0.51	0.48
Nd	0.88	0.84	1.16	1.25	4.42	4.34	2.99	3.57	3.34	3.22	1.92	1.8
Sm	0.09	0.08	0.16	0.13	0.37	0.38	0.35	0.24	0.25	0.27	0.26	0.18
Eu	0.35	0.75	0.41	0.39	0.89	0.96	0.81	0.72	0.8	0.54	0.51	0.44
Gd	<0.10	0.12	0.12	0.1	0.25	0.26	0.23	0.15	0.23	0.12	0.1	0.17
Tb	<0.01	0.01	<0.01	0.01	0.02	<0.01	0.02	<0.01	0.01	<0.01	<0.01	0.01
Dy	0.05	0.04	0.03	0.04	0.06	<0.05	0.08	0.1	0.06	<0.04	<0.06	0.05
Ho	<0.01	<0.01	<0.01	0.01	0.01	0.02	<0.01	0.02	0.01	<0.01	<0.01	<0.01
Er	<0.02	<0.02	<0.02	<0.03	0.04	<0.02	<0.05	0.04	0.04	<0.03	<0.03	<0.03
Tm	<0.01	<0.01	<0.01	0.01	0.01	<0.01	<0.01	<0.01	<0.01	<0.01	<0.01	<0.01
Yb	<0.07	<0.04	<0.06	<0.04	<0.08	0.04	0.06	<0.06	<0.04	<0.05	<0.06	<0.05
Lu	0.01	<0.01	<0.01	<0.01	<0.01	<0.01	<0.01	0.01	<0.01	<0.01	<0.01	<0.01
Hf	<0.03	0.04	<0.03	<0.03	<0.02	<0.02	<0.03	<0.05	<0.02	<0.02	<0.05	0.02
Ta	<0.06	<0.01	<0.01	<0.01	<0.01	<0.01	<0.01	<0.01	<0.01	0.01	0.01	<0.01
Pb	0.2	0.21	0.51	0.55	1.03	1.03	1.28	0.85	1.04	0.71	0.52	0.46
Th	<0.02	<0.01	<0.01	0.02	<0.03	<0.01	<0.02	<0.02	<0.01	0.04	<0.02	<0.01
U	<0.01	<0.01	<0.01	<0.01	0.01	<0.01	<0.02	<0.01	<0.01	0.02	<0.02	<0.01

Tab. 5

Representative LA-ICP-MS data for core and rim of selected plagioclases (wt.% for major and ppm for trace elements).

5. Discussion

5.1. Evolution of Mt. Etna's phases over time

From the whole-rock bivariate major and trace element diagrams (Figures 4 and 5) it is evident that the alkali basalts of the various phases show large differences over time. With some exceptions, the majority of these samples display a trend line in the various major oxide versus mg# plots (Figure 4) but without reflecting a correlation between fractionation and time of eruption. Older more fractionated and younger more primitive compositions as well as older more primitive and younger more fractionated compositions occur at Mt. Etna.

Sample	BT-A Basal Tholeiitic		T-SG Timpe		VB-VSG Valle del Bove		E-R Ellittico		M-1669 Mongibello		M-2013 Mongibello	
	Core	Rim	Core	Rim	Core	Rim	Core	Rim	Core	Rim	Core	Rim
SiO ₂	39.90	37.00	37.27	36.15	37.18	38.91	38.06	37.42	37.35	36.71	36.77	36.24
Al ₂ O ₃	0.05	0.04	0.02	0.03	<0.05	<0.05	<0.05	<0.05	0.06	0.13	0.04	<0.05
FeO	14.77	29.35	24.66	30.04	28.47	22.51	23.63	27.85	23.65	28.47	25.45	25.99
MnO	0.20	0.40	0.38	0.56	0.81	0.53	0.66	0.84	0.43	0.65	0.41	0.52
MgO	45.19	33.00	37.52	33.01	33.21	38.15	36.88	33.26	37.89	33.86	36.41	36.53
CaO	0.21	0.33	0.22	0.28	0.28	0.22	0.21	0.20	0.34	0.39	0.35	0.41
Total	100.32	100.12	100.07	100.07	99.95	100.32	99.44	99.57	99.72	100.21	99.43	99.69
Li	1.85	2.07	3.04	2.86	4.64	6.19	8.21	8.34	3.44	4.39	3.87	4.57
Ti	45	56.1	52.5	119	80.6	81.1	107	118	101	104	76.7	83.2
V	5.16	9.31	5.43	7.57	2.68	2.61	3.97	3.43	5.64	6.56	4.94	5.36
Cr	341	239	4.55	8.83	<0.65	<0.63	<0.72	<0.87	3.12	2.94	<0.61	<0.65
Mn	1376	1497	2996	2207	3738	4382	5067	5139	2770	3280	2955	3644
Co	201	193	233	232	204	209	154	154	221	223	213	213
Ni	2330	1379	554	570	168	147	3.43	2.56	357	320	204	202
Cu	1.29	1.41	3.35	3.12	2.57	2.87	0.88	0.55	5.38	6.69	7.76	8.29
Zn	160	161	229	251	316	386	335	334	221	256	255	258

Tab. 6

Representative LA-ICP-MS data for core and rim of selected olivines (wt.% for major and ppm for trace elements).

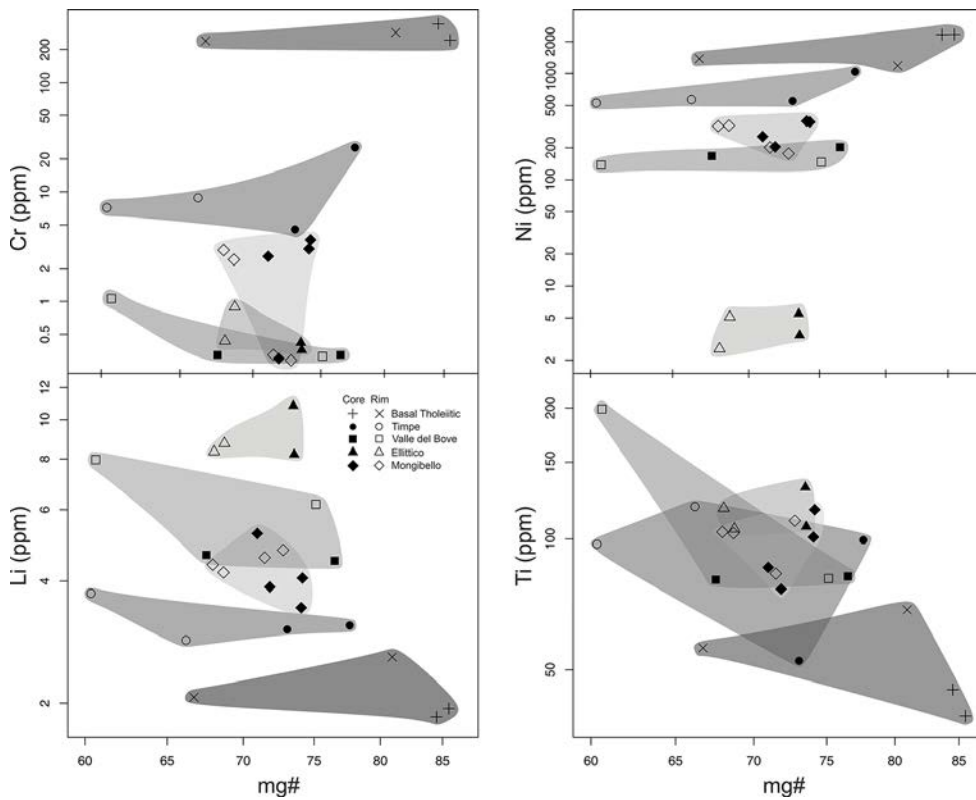


Fig. 9

Bivariate diagram of olivine core and rim ICP-MS analyses. Trace elements Cr, Ni, Li and Ti are plotted against X_{Mg} which is used as fractionation index.

Sample	BT-A		T-SG		VB-VSG		E-R		M-1669		M-2013	
	Basal Tholeiitic		Timpe		Valle del Bove		Ellittico		Mongibello		Mongibello	
	Core	Rim	Core	Rim	Core	Rim	Core	Rim	Core	Rim	Core	Rim
SiO ₂	52.85	52.61	50.13	50.63	51.72	49.86	50.86	50.76	51.22	49.55	50.38	49.64
TiO ₂	0.54	0.70	1.17	1.21	0.66	1.25	1.29	1.50	1.34	1.87	1.02	1.66
Al ₂ O ₃	2.04	1.24	3.85	3.34	3.10	4.64	3.80	4.47	3.66	4.30	4.94	5.31
Cr ₂ O ₃	0.50	<0.05	0.04	<0.05	<0.05	0.02	0.07	0.04	0.05	0.07	0.07	0.03
FeO	6.01	10.21	8.36	9.04	6.51	7.27	7.87	8.22	8.11	9.02	7.74	8.49
MnO	0.18	0.26	0.10	0.23	0.18	0.18	0.23	0.23	0.13	0.22	0.09	0.17
MgO	16.36	16.15	14.14	13.89	15.08	13.97	14.47	14.38	14.53	13.19	14.49	13.19
CaO	20.37	18.37	21.30	21.44	22.42	22.13	20.92	20.62	20.88	20.93	20.96	21.27
Na ₂ O	0.31	0.28	0.58	0.52	0.47	0.53	0.41	0.38	0.48	0.52	0.4	0.44
K ₂ O	<0.05	<0.05	<0.05	<0.05	<0.05	<0.05	<0.05	<0.05	<0.05	<0.05	<0.05	<0.05
Total	99.16	99.82	99.67	100.30	100.14	99.85	99.92	100.60	100.40	99.67	100.09	100.20
Li	6.4	9.4	6.52	21.1	3.34	11.7	22	30.3	0.8	2.7	1.71	1.17
Be	0.1	<0.04	0.16	0.31	0.49	0.53	0.46	0.33	0.19	0.11	0.37	0.27
Ti	4726	4863	10229	8536	8642	9235	8900	7751	8773	9281	8668	9012
V	458	544	442	402	227	213	277	244	404	388	299	355
Cr	4701	389	119	490	<0.73	4.76	<0.77	<0.65	44.9	94.1	311	30.5
Mn	1193	1519	1740	1458	1866	1668	2006	2015	1793	1438	1712	1405
Co	47	58.2	45.1	46	36.4	36.7	36	32.5	48.1	44.6	44	44.3
Ni	146	95	64.6	101	13.9	21.2	2.85	1.85	53.2	48.8	55.3	45.7
Cu	12.8	2.33	4.01	42.5	1.89	2.76	6.35	2.01	2.53	4.72	4.25	2.68
Zn	55	73.5	70	52.3	66.3	58.3	70	65.9	64.7	53.1	50.1	53
Ga	9.87	4.05	13.6	14.3	14.1	13.8	15.8	11.7	14.2	13	11.8	18.1
Ge	2.5	2.32	3.24	2.38	2.6	2.49	2.65	2.77	2.78	2.54	2.65	2.34
Rb	0.16	<0.06	<0.09	0.23	<0.11	<0.10	0.14	<0.10	<0.09	<0.09	<0.10	<0.09
Sr	131	25.8	81.9	78	169	157	134	141	113	112	158	128
Y	13.1	17	26.5	21	51.3	35.8	38.4	35.8	31.9	29.2	21.6	28.8
Zr	24.2	13.4	75	57.1	250	191	162	112	151	123	61.9	167
Nb	0.43	0.08	0.74	0.55	1.82	1.43	1.3	0.79	0.96	0.88	0.54	0.96
Cs	<0.07	<0.05	<0.08	<0.09	<0.10	<0.10	<0.10	<0.09	<0.09	<0.08	<0.10	<0.10
Ba	14	0.66	<0.08	0.61	<0.07	<0.11	2.32	0.12	0.52	0.48	<0.08	<0.08
La	2.77	1.66	8.66	5.81	29.5	20.2	22.2	17.3	17.9	13.8	8.45	17.1
Ce	7.52	5.12	30.2	18.2	87.7	60.6	65.3	54.5	57.5	43.5	33	48.1
Pr	1.27	1.3	4.67	2.98	15	10.2	9.94	9.29	8.61	7.48	5.35	6.62
Nd	8.66	7.58	25.8	20.4	82.6	58.1	67.7	53.3	48.3	38.8	27.6	49.4
Sm	2.45	2.03	7.8	5.55	18.7	13.3	15.8	13.1	12.3	9.85	8.38	12.3
Eu	0.87	0.79	2.04	1.53	4.82	3.66	3.7	3.32	2.75	2.72	2.34	2.57
Gd	3.31	3.54	7.62	6.04	18.4	12.7	15.4	12.3	10.4	9.25	6.42	11.8
Tb	0.52	0.4	1.25	0.88	2.28	1.53	2.06	1.62	1.47	1.21	0.95	1.63
Dy	2.88	3.36	6.28	4.41	12.2	8.12	8.97	8.42	6.61	6.65	5.15	6.7
Ho	0.61	0.68	1.2	0.98	2.23	1.54	1.85	1.57	1.32	1.22	0.84	1.35
Er	1.58	1.31	3.45	2.46	5.22	3.71	4.85	3.7	3.42	2.9	2.14	3.9
Tm	0.16	0.22	0.38	0.28	0.62	0.43	0.45	0.41	0.39	0.36	0.27	0.38
Yb	1.23	1.57	2.49	1.85	4.01	2.93	3.4	2.96	2.6	2.29	1.62	2.67
Lu	0.19	0.13	0.36	0.29	0.53	0.4	0.5	0.39	0.41	0.29	0.21	0.41
Hf	0.79	0.7	2.92	1.89	7.75	6.15	5.43	4.44	4.87	4.55	2.83	4.51
Ta	0.03	0.01	0.09	0.08	0.31	0.3	0.21	0.13	0.13	0.15	0.06	0.14
Pb	0.14	0.02	0.09	0.08	0.16	0.11	0.14	0.11	0.14	0.1	0.1	0.1
Th	0.09	0.02	0.1	0.06	0.35	0.24	0.27	0.16	0.19	0.2	0.13	0.22
U	0.02	<0.01	0.02	0.02	0.06	0.04	0.07	0.03	0.03	0.03	0.02	0.03

Tab. 7

Representative LA-ICP-MS data for core and rim of selected clinopyroxenes (wt.% for major and ppm for trace elements).

These differences clearly indicate that changes in the magma chamber/s of Mt. Etna occurred. Processes leading to such changes may be mainly attributed to fractional crystallisation and input of more primitive magmas, latter one mixing and substituting already more evolved/differentiated melts in the magma chamber/s and/or contamination from crustal rocks. CORSARO & POMPILIO (2004) suggested that a multi-stage fractional crystallisation of phenocryst-forming minerals is the decisive factor for the evolutionary differentiation of recent Etnean magmas. However, as Mt. Etna is located in a complicated geological setting, changes that led to compositional differences in the erupted Etnean magmas can be related also to processes in the magma source.

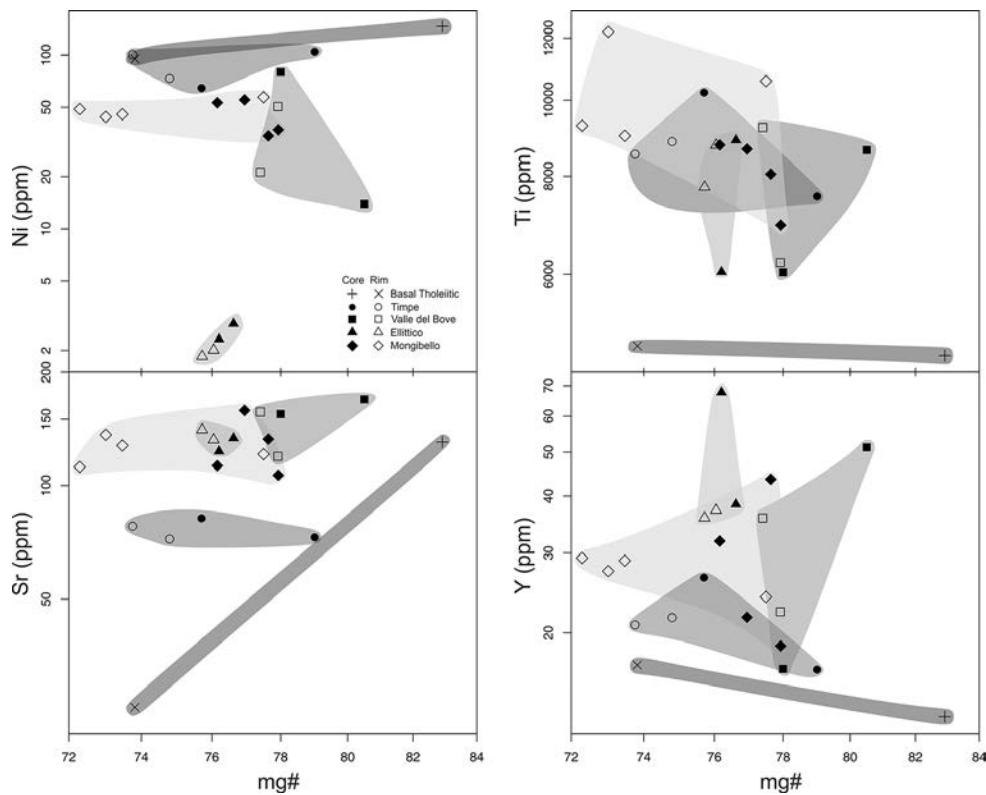


Fig. 10

Bivariant diagram of clinopyroxene core and rim ICP-MS analyses. Trace elements Ni, Ti, Sr and Y are plotted against X_{Mg} which is used as fractionation index.

This change between more primitive and more fractionated and possibly contaminated rock compositions is also reflected by the trace element content of the minerals plagioclase, olivine and clinopyroxene (Figures 8 to 10). For plagioclase (Figure 8) the content of the elements Sr and Ba reflect the degree of evolution of the magma or contamination at the stage of crystallisation of these phenocrysts. Sr is usually an incompatible element for most minerals but is incorporated into plagioclase. Thus higher Sr contents in plagioclase are interpreted as to be derived either from a highly enriched/contaminated magma or is a measure of more evolved basalts. A few plagioclase phenocrystals also show an increase in anorthite component from core to rim (Figure 8) as they started to crystallize in a higher fractionated liquid while the rims grew with input of a fresher and less evolved magma. In the case of olivine (Figure 9) Li is regarded as an incompatible element and shows different concentrations with increasing fractionation with the highest Li content in the Ellittico olivines meaning that at the time of crystallisation of these crystals the liquid was highly enriched in Li. The absolute low concentrations of the compatible element Ni in olivine grains of the E-R sample (Ellittico) also indicate a highly fractionated liquid with high depletion of this element. Low Ni content is also observed in clinopyroxene of the same sample E-R and can be explained as above. The overall trend of trace elements in clinopyroxene phenocrystals is shown in Figure 10, which displays differences between cores and rims.

5.2. Tectonic position

Compositional similarities of the analysed Etnean samples with the Hawaiian volcanoes Kilauea, Mauna Kea and Mauna Loa are notable. Hawaiian volcanoes are hot spot (intraplate) volcanoes and clearly display a within-plate tectonic position. For Mt. Etna's erupted products the discrimination diagram by PEARCE (1982) shows that, starting from the Timpe phase onwards when composition changed from tholeiitic to alkaline, the volcano displays a within-plate signature, just like the Hawaiian volcanoes. The fact that the samples show a within-plate basalt affinity (ocean island basalt) would be in line with the hypothesis of an intraplate volcano. According to ARMIENTI et al. (1989) the within-plate basalt signature appears distinctly for the Etnean alkaline rocks. However, Mt. Etna volcano is located above a convergent plate margin between the African plate and the Eurasian plate (CORREALE et al., 2014) but does not show a typical volcanic/island-arc signature. According to DOGLIONI et al. (2001) Mt. Etna is located close to the subduction zone in the hanging wall of the accretionary wedge. Further, a N-S oriented compressional setting, present in this tectonically active zone, influences the Etnean edifice (LANZAFAME et al., 1997).

Thus we have the unusual situation where eruption products with a within-plate basalt affinity are located in a subductional environment. This could mean that Mt. Etna volcano is a hot spot fed volcano located in a subductional environment. As stated by CORSARO & CRISTOFOLINI (1996) the magma source of Mt. Etna reflects characteristics of an intraplate volcano if contamination by the subductional environment is excluded. The analysed samples however display some possible contamination by the underlying crust as seen by the Sr and Pb peaks in Figure 6. Further, CRISTOFOLINI et al. (1987) stated that there is a subduction-related geochemical imprint on Mt. Etna's eruption products. This indicates that the overall tectonic situation in the Etnean environment is complicated. An assumption would be that within-plate characteristics are inherited directly from the magma source. As the volcano is located close to the subduction zone, contamination by crustal rocks or sediments is achieved during magma residence in the magma chamber/s. Mt. Etna's plumbing system features a multi-level magma reservoir where magma is stored at depths of 6.5, 2 and 0 km (ALOISI et al., 2011) meaning that contamination could happen at different depths.

5.3. Magmatic source

The magma source of old and recent eruptions is regarded to derive from an already slightly depleted garnet lherzolite by 1% of melting (CORSARO & CRISTOFOLINI, 1996). This fact would be in line with the degree of melting necessary for generating the alkali basalts but can not fully explain the various geochemical and isotopic signatures of the erupted products (VICCARO & CRISTOFOLINI, 2008). REE chondrite (NAKAMURA, 1974) normalised whole rock compositions display enrichment of LREE over HREE (Figure 11). The explanation for the depletion of HREE may be related to HREE retention by a garnet lherzolite. The amount of HREE depletion in basalts can be used as simple depth indicator from where the magma comes: Lherzolites in the upper mantle have spinel stable from around 30 to 80 km and 9 to 24 kbar respectively, whereas lherzolites in deeper depths starting from approximately 80 km (around 24 kbar) onwards contain garnet, which incorporates HREE. Therefore, melts of basalts showing depletion in HREE may have originated in great depth having as source a garnet lherzolite (GILL, 2010).

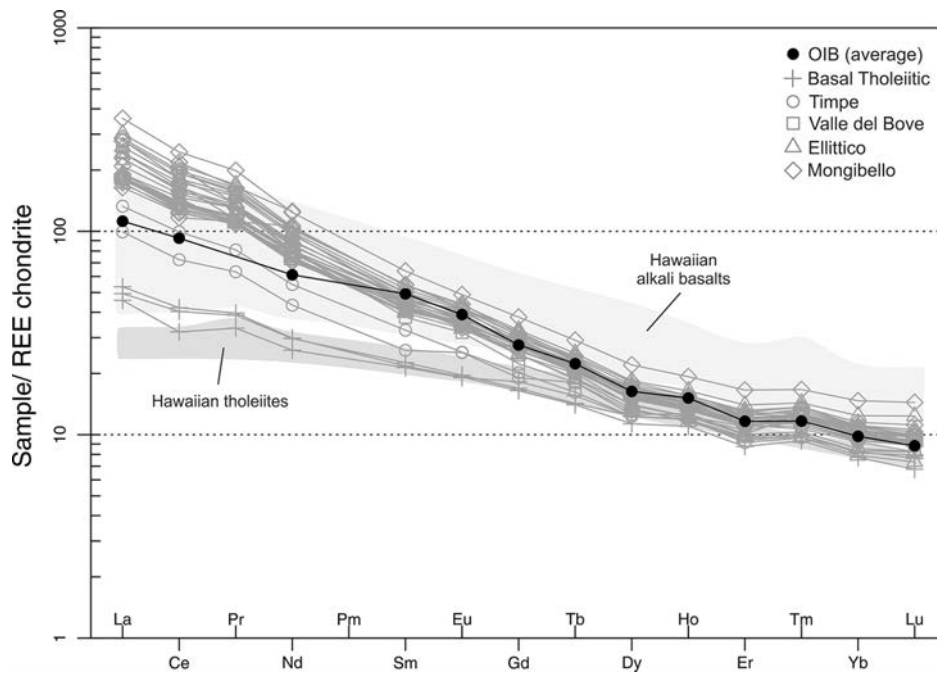


Fig. 11
 NAKAMURA (1974) REE chondrite normalized plot of representative samples compared with a typical average within-plate basalt (SUN & MCDONOUGH, 1989) as well as selected tholeiitic and alkali basaltic compositions of Hawaiian volcanoes.

6. Conclusion

Within the framework of the present study, Mt. Etna samples from selected lava flows ranging from the first fissure type eruptions to the latest Strombolian activity were mineralogically, petrologically and geochemically investigated with the main focus on geochemistry.

a. The samples of the Basal Tholeiitic phase represent the most primitive compositions of Mt. Etna's eruption products. They are subsequently followed by the more evolved alkaline compositions which however do not display increasing chemical fractionation and do not reflect steady continuing evolution of the liquid over time as the compositions of the erupted products fluctuate from chemically evolved to less evolved/more primitive and vice versa.

b. The compositions of the alkali basalts suggest that mainly fractional crystallisation and input of more primitive magma into the feeding system of Mt. Etna volcano played a significant role in the differentiation of the samples. It is also important to note that the magma source also plays a part in the geochemical characteristics of the erupted products.

c. Mt. Etna's erupted products have a within-plate basalt signature and show similarities with the Hawaiian volcanoes. This clearly indicates that Mt. Etna volcano is a hot spot fed volcano located in a subductional environment where its eruption products also feature possible crustal contamination, as seen by trace element distributions.

Acknowledgements

We wish to thank Prof. Aberra Mogessie for his advise and helpful contributions during the writing of this paper. E.B. is also thankful for his supervision during his master thesis. Special thanks to Dr. Stefano Branca, National Institute of Geophysics and Volcanology (INGV) of Catania in Sicily, for his support during the sample acquisition on Mt. Etna.

References

- ALOISI, M., MATTIA, M., FERLITO, C., PALANO, M., BRUNO, V. & CANNAVÒ, F. (2011): Imaging the multi-level magma reservoir at Mt. Etna volcano (Italy). - *Geophys. Res. Lett.*, 38
- ARMIENTI, P., INNOCENTI, F., PETRINI, R., POMPILIO, M. & VILLARI, L. (1989): Petrology and Sr-Nd isotope geochemistry of recent lavas from Mt. Etna: bearing on the volcano feeding system. - *J. Volcanol. Geotherm. Res.*, 39, 315-327
- BEHNKE, B. & DE BENI, E. (2014): Rapporto UFVG 22.01.2014, INGV Catania
- BRANCA, S., COLTELLI, M. & GROPELLI, G. (2004): Geological evolution of Etna volcano. - In: *Etna Volcano Laboratory*, Bonaccorso A., Calvari S., Coltelli M., Del Negro C., Falsaperla S. (Eds.), AGU (Geophysical monograph series), 143, 49-63
- BRANCA, S., COLTELLI, M. & GROPELLI, G. (2011): Geological evolution of a complex basaltic stratovolcano: Mount Etna, Italy. - *It. J. Geosci. (Boll. Soc. Geol. It.)*, 130, 306-317
- BUSÀ, T., CLOCCHIATTI, R. & CRISTOFOLINI, R. (2002): The role of apatite fractionation and REE distribution in alkaline rocks from Mt. Etna, Sicily. - *Mineral. Petrol.*, 74, 95-114
- CLOCCHIATTI, R., CONDOMINES, M., GUÈNOT, N. & TANGUY, J.C. (2004): Magma changes at Mount Etna: The 2001 and 2002-2003 eruptions. - *Earth Planet. Sci. Lett.*, 226, 397-414
- CORREALE, A., PAONITA, A., MARTELLI, M., RIZZO, A., ROTOLO, S.G., CORSARO, R.A. & DI RENZO, V. (2014): A two-component mantle source feeding Mt. Etna magmatism: Insights from the geochemistry of primitive magmas. - *Lithos*, 184-187, 243-258
- CORSARO, R.A. & CRISTOFOLINI, R. (1996): Origin and differentiation of recent basaltic magmas from Mount Etna. - *Mineral. Petrol.*, 57, 1-21
- CORSARO, R.A. & POMPILIO, M. (2004): Dynamics of magmas at Mount Etna. - In: *Etna Volcano Laboratory*, Bonaccorso A., Calvari S., Coltelli M., Del Negro C., Falsaperla S. (Eds.), AGU (Geophysical monograph series), 143, 91-110
- CRISTOFOLINI, R. (1972): Tholeiitic basalts from Etna. - *Per. Mineral.*, 41, 167-200
- CRISTOFOLINI, R., MENZIES, M.A., BECCALUVA, L. & TINDLE, A. (1987): Petrological notes on the 1983 lavas at Mount Etna, Sicily, with reference to their REE and Sr-Nd isotope composition. - *Bull. Volcanol.*, 49, 599-607
- DEL CARLO, P., BRANCA, S., DE BENI, E., LO CASTRO, M.D. & WJBRANS, J.R. (2012): The Mt. Moio eruption (Etna): Stratigraphy, petrochemistry and $^{40}\text{Ar}/^{39}\text{Ar}$ age determination with inferences on the relationship between structural setting and magma intrusion. - *J. Volcanol. Geotherm. Res.*, 241-242, 49-60
- DI STEFANO, A. & BRANCA, S. (2002): Long-term uplift rate of the Etna volcano basement (southern Italy) based on bio-chronological data from Pleistocene sediments. - *Terra Nova*, 14, 61-68
- DOGLIONI, C., INNOCENTI, F. & MARIOTTI, G. (2001): Why Mt Etna? - *Terra Nova*, 13, 25-31
- GILL, R. (2010): *Igneous rocks and processes*. - Wiley-Blackwell Publishing
- LANZAFAME, G., NERI, M., COLTELLI, M., LODATO, L. & RUST, D. (1997): North-South compression in the Mt. Etna region (Sicily): Spatial and temporal distribution. - *Acta Vulcanol.*, 9, 1-2, 121-133

- LE BAS, M.J., LEMAITRE, R.W., STRECKEISEN, A. & ZANETTIN, B. (1986): A chemical classification of volcanic rocks based on the Total Alkali Silica diagram. - *J. Petrol.*, 27, 3, 745-750
- LOPEZ, M., POMPILIO, M. & ROTOLO, S.G. (2006): Petrology of some amphibole-bearing volcanics of the pre-Elittico period (102-80 ka), Mt. Etna. - *Per Mineral.*, 75, 151-166
- MARSKE, J.P., GARCIA, M.O., PIETRUSZKA, A.J., RHODES, J.M. & NORMAN, M.D. (2008): Geochemical Variations during Kilauea's Pu'u 'O'o Eruption Reveal a Fine-scale Mixture of Mantle Heterogeneities within the Hawaiian Plume. - *J. Petrol.*, 49, 7, 1297-1318
- MÈTRICH, N., ALLARD, P., SPILLAERT, N., ANDRONICO, D. & BURTON, M. (2004): 2001 flank eruption of the alkali- and volatile-rich primitive basalt responsible for Mount Etna's evolution in the last three decades. - *Earth Planet. Sci. Lett.*, 228, 1-17
- NAKAMURA, N. (1974): Determination of REE, Ba, Fe, Mg, Na, and K in carbonaceous and ordinary chondrites. - *Geo. Cosm. Acta*, 38, 5, 757-775.
- NICOTRA, E. & VICCARO, M. (2012): Unusual magma storage conditions at Mt. Etna (Southern Italy) as evidenced by plagioclase megacryst-bearing lavas: Implications for the plumbing system geometry and summit caldera collapse. - *Bull. Volcanol.*, 74, 795-815
- PARESCHI, M.T., CAVARRA, L., INNOCENTI, F. & PASQUARÈ, G. (1999): Digital Atlas of Mt Etna volcano. - *Acta Vulcanol.*, 11, 2
- PEARCE, J.A. (1982): Trace element characteristics of lavas from destructive plate boundaries. - In: Thorpe R.S. (ed.) *Andesites: Orogenic Andesites and Related Rocks*. John Wiley and sons, Chichester, 525-548
- ROLLINSON, H. (1993): Using geochemical data: evaluation, presentation, interpretation. - Longman scientific and technical, 352 pp
- SISSON, T.W., KIMURA, J.I. & COOMBS, M.L. (2009): Basanite–nephelinite suite from early Kilauea: carbonated melts of phlogopite–garnet peridotite at Hawaii's leading magmatic edge. - *Contrib. Mineral. Petrol.*, 158, 6, 803-829
- SUN, S.S. & MCDONOUGH, W.F. (1989): Chemical and isotopic systematics of oceanic basalts: implications for mantle composition and processes. - *Geol. Soc. London, Special Publications*, 42, 313-345
- TANGUY, J.C., CONDOMINES, M. & KIEFFER, G. (1997): Evolution of the Mount Etna magma: Constraints on the present feeding system and eruptive mechanism. - *J. Volcanol. Geotherm. Res.*, 75, 221-250
- VICCARO, M. & CRISTOFOLINI, R. (2008): Nature of mantle heterogeneity and its role in the short-term geochemical and volcanological evolution of Mt. Etna (Italy). - *Lithos*, 105, 272-288
- WANG, H.J., FREY, F.A., GARCIA, M.O. & CLAGUE, D.A. (1994): Submarine lavas from Mauna Kea Volcano, Hawaii: Implications for Hawaiian shield stage processes. - *J. Geophys. Res. Solid Earth*, 99, B8, 15577–15594
- WANLESS, V.D., GARCIA, M.O., RHODES, J.M., WEIS, D. & NORMAN, M.D. (2006): Shield-stage alkalic volcanism on Mauna Loa Volcano, Hawaii. - *J. Volcanol. Geotherm. Res.*, 151, 141-155
- WEST, H.B., GARCIA, M.O., FREY, F.A. & KENNEDY, A. (1988): Nature and cause of compositional variation among the alkalic cap lavas of Mauna Kea Volcano, Hawaii. - *Contrib. Mineral. Petrol.*, 100, 383-397

received: 03.05.2016

accepted: 15.05.2016